A data assimilation method for using low-resolution Earth observation data in heterogeneous ecosystems

T. C. Hill,[1] T. Quaife,[2] and M. Williams[1]

Received 29 October 2010; revised 4 February 2011; accepted 8 February 2011; published 29 April 2011.

[1] We present an approach for dealing with coarse-resolution Earth observations (EO) in terrestrial ecosystem data assimilation schemes. The use of coarse-scale observations in ecological data assimilation schemes is complicated by spatial heterogeneity and nonlinear processes in natural ecosystems. If these complications are not appropriately dealt with, then the data assimilation will produce biased results. The "disaggregation" approach that we describe in this paper combines frequent coarse-resolution observations with temporally sparse fine-resolution measurements. We demonstrate the approach using a demonstration data set based on measurements of an Arctic ecosystem. In this example, normalized difference vegetation index observations are assimilated into a "zero-order" model of leaf area index and carbon uptake. The disaggregation approach conserves key ecosystem characteristics regardless of the observation resolution and estimates the carbon uptake to within 1% of the demonstration data set "truth." Assimilating the same data in the normal manner, but without the disaggregation approach, results in carbon uptake being underestimated by 58% at an observation resolution of 250 m. The disaggregation method allows the combination of multiresolution EO and improves in spatial resolution if observations are located on a grid that shifts from one observation time to the next. Additionally, the approach is not tied to a particular data assimilation scheme, model, or EO product and can cope with complex observation distributions, as it makes no implicit assumptions of normality.

Citation: Hill, T. C., T. Quaife, and M. Williams (2011), A data assimilation method for using low-resolution Earth observation data in heterogeneous ecosystems, *J. Geophys. Res.*, *116*, D08117, doi:10.1029/2010JD015268.

1. Introduction

[2] Understanding the spatial and temporal variability of terrestrial ecosystem states and processes remains an important challenge. Complexity in the Earth system derives in large part from the interactions between ecological and environmental processes over a range of temporal and spatial scales. Naturally occurring ecosystems systems often tend to vary continuously rather than discretely [*Fletcher et al.*, 2009] and the length scales for these variations do not necessarily match the scales of observation. Furthermore, because interactions are nonlinear in many biophysical systems [*Jarvis*, 1995], the use of mean states can lead to large biases in expected ecosystem response [*Chen et al.*, 2007; *Kimball et al.*, 1999]. *Chen et al.* [2007] showed differences of up to 25% (5% to 15% average) in simulations of Canada's surface carbon fluxes based on averaged remotely sensed parameter versus "fine scale" (1 km^2) parameters. *Stoy et al.* [2009] showed that by spatially averaging ecosystem properties, rather than preserving a probability density function (PDF), the resulting biases will change the predicted response from a moderate sink of carbon into a source of equal magnitude.

[3] Thus our current understanding of ecosystem dynamics and land-atmosphere interactions is at least partially limited by data availability and resolution. This is largely because critical processes operate on a range of spatial and temporal scales [*Jarvis*, 1995]. Land surfaces tend to be highly heterogeneous and so direct measurements frequently undersample, or average out, the variability. Additionally, biophysical interactions are nonlinear and require complex monitoring. Satellite observations can help address many of these issues, but have temporal/spatial resolution trade-offs. Inherently, satellites with global coverage have either, fine spatial resolution observations and a lower return frequency (e.g., Landsat and IKONOS); or frequent observations and a coarse spatial resolution (e.g., MODIS and AVHRR). It should also be noted that, satellite derived reflectance does not scale linearly with many of the ecosystem properties it is used to measure, for example, the relationship between normalized difference vegetation index (NDVI) and leaf area index (LAI) [*Chen*, 1999; *van Wijk*

[1]School of GeoSciences and NERC National Centre for Earth Observation, University of Edinburgh, Edinburgh, UK.
[2]School of Geography and NERC National Centre for Earth Observation, University of Exeter, Cornwall, UK.

0148-0227/11/2010JD015268

and Williams, 2005]. Therefore, we must properly account for scaling issues if we are to make use of satellite observations and avoid introducing biases.

[4] Work has been done to combine plot studies with multisatellite data, for example to extrapolate biomass estimates over the Amazon basin at 1 km [*Saatchi et al.*, 2007]. The technique combines the accurate measurements of the plots with the spatial coverage of remote sensing to provide a snap shot of biomass with uncertainty. However, the approach presented by *Saatchi et al.* [2007] ignored information formalized in process based ecosystem models. Both *Demarty et al.* [2007] and *Tang and Zhuang* [2008] use data assimilation to improve the simulation of spatially explicit biosphere processes, though neither study deals with the critical issue of biased data assimilation analyses due to scaling problems.

[5] Data assimilation has been successfully used to combine ecosystem models with time series satellite observations at particular sites [*Quaife et al.*, 2008; *Tang and Zhuang*, 2009; *Zobitz et al.*, 2008]. However, a generalized approach for combining direct measurements and satellite observations with arbitrary spatial resolutions is still missing [*Raupach et al.*, 2005]. *Tang and Zhuang* [2008] call for an integrated model-data fusion scheme to reduce the impact of "equifinality" in ill-posed problems. Implicit to the approach of reducing equifinality with multiple orthogonal data, is the issue of scaling. Clearly, if the effects of scaling outlined in multiple studies [*Chen et al.*, 2007; *Chen*, 1999; *Kimball et al.*, 1999; *Stoy et al.*, 2009] are not accounted for, then using multiresolution observations in non linear systems will lead to confused results, and will not help address the equifinality of ill-posed inversions.

[6] In this manuscript we present a new and flexible approach to spatial data assimilation. We avoid the problems of scaling by combining coarse-resolution EO with a probability distribution function (PDF) which describes the subpixel spatial heterogeneity. This PDF must capture the natural heterogeneity at a sufficiently fine resolution to preserve critical ecosystem states and processes. The coarse EO is disaggregated so it maintains the high-resolution spatial information from the model state, the mean properties of the coarse observation and is combined with an estimate of the observation's PDF to create a new, fine-resolution observation. This new disaggregated observation can then be assimilated normally, and thus can be applied easily to most sequential data assimilation approaches. The approach allows great flexibility in combining both high and low, spatial and temporal resolution observations within a data assimilation scheme to provide an unbiased estimate of ecosystem states and processes. Using a demonstration set of normalized difference vegetation index (NDVI) observations we demonstrate the potential of this approach to constrain estimates of carbon uptake over a 512 m by 512 m area. To do this we address a number of questions: (1) To what degree does the standard data assimilation of coarse observations introduce bias? (2) Does the disaggregation approach perform better than the standard data assimilation? (3) How does the disaggregation perform with more complex observations: First, with combinations of coarse spatial resolution (high frequency) and fine spatial resolution (infrequent) observations? Second, with observation aligned on a grid that moves between observations times?

2. Methods

2.1. Sequential Data Assimilation and the Particle Filter

[7] Sequential data assimilation approaches are particularly useful in ecological applications, where they have been successfully applied to both state and parameter estimation [*Quaife et al.*, 2008; *Williams et al.*, 2005]. In common with other data assimilation schemes, sequential filters and smoothers are based on the application of *Bayes* [1763] theory. However, unlike variational data assimilation methods that rely on gradient descent algorithms for efficiency, most sequential methods do not require a model adjoint (the Extended Kalman Filter being a notable exception to this), so the implementation of sequential methods with an arbitrary ecosystem model is typically far simpler. However, the relative merits of each approach are often situation dependent and have been much discussed in the literature [*Raupach et al.*, 2005; *Williams et al.*, 2009]. The approach that we describe in this paper is independent of the specific data assimilation implementation chosen.

[8] In this study we implement a Monte Carlo Metropolis-Hastings sequential particle filter [*Dowd*, 2007]. This particle filter was chosen for its simple implementation and numerical efficiency and ability to use a nonlinear model operator. *van Leeuwen* [2009] provides a detailed review of the different particle filtering approaches. The Ensemble Kalman Filter (EnKF) [*Evensen*, 2003, 2009] is another common sequential data assimilation approach used in ecological studies. For the purposes of this study it is a somewhat arbitrary choice between the two approaches, and we would not expect using the EnKF to alter the conclusions of this study. However, while the EnKF has been applied with considerable success in a wide range of nonlinear systems, it should be noted that the EnKF does not explicitly allow for nonlinear model operators. The ability of the particle filter to explicitly deal with nonlinear models and arbitrary model operators is highly beneficial when considering the complex and nonlinear processes of terrestrial ecosystems.

2.2. Disaggregation Approach

[9] Satellite observations with good spatial coverage and regular sampling are an obvious data stream for use in ecological data assimilation schemes. However, the spatial resolution of temporally frequent satellite observations can be coarse (e.g., MODIS has a resolution of 250 to 1000 m) in comparison to the critical scales (on the order of meters) of many terrestrial ecosystem processes [*Spadavecchia et al.*, 2008]. This disparity in scales creates problems for data assimilation schemes. *Stoy et al.* [2009] showed that merely preserving the mean state of an ecosystem parameter was not sufficient to preserve an accurate representation of the processes within an ecosystem model. Indeed to preserve the response the mean, variance and skew need to be preserved. The approach that we describe in this manuscript provides a general framework for consistently combining observations with a wide range of spatial and temporal resolutions and extents, while preserving the PDF of the

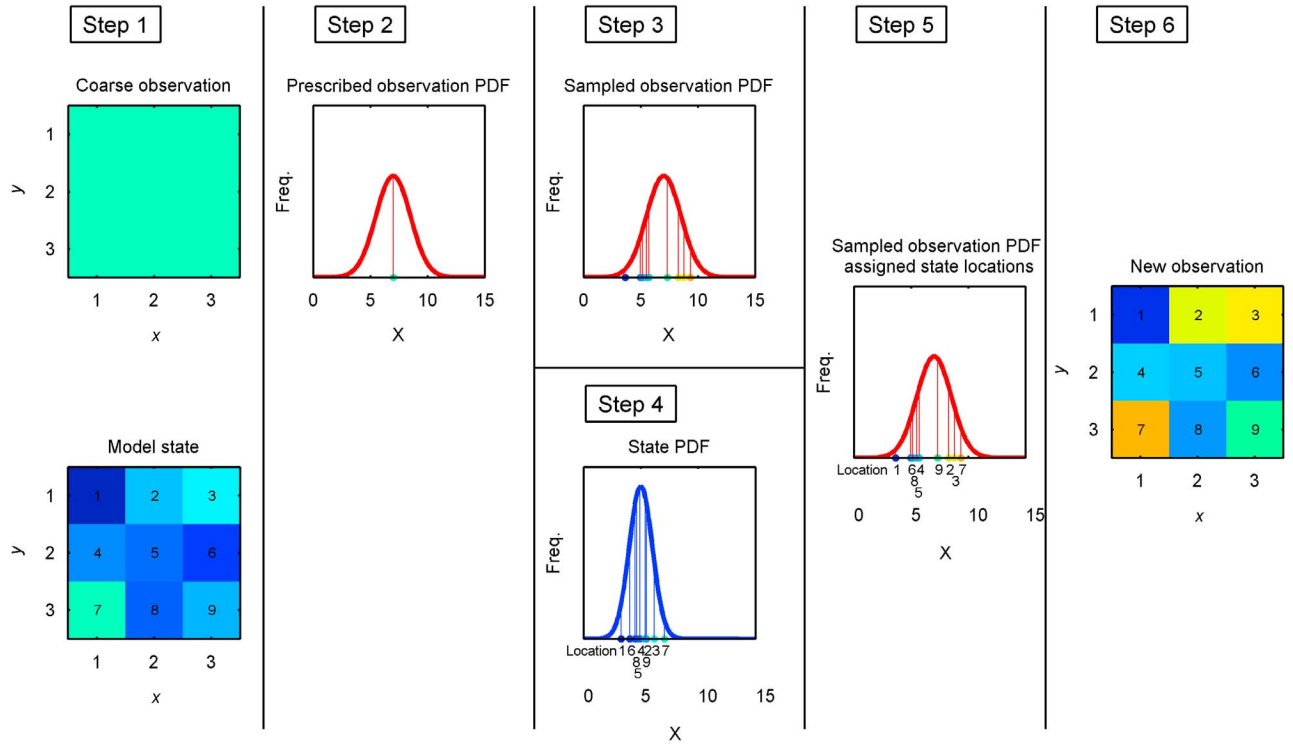

Figure 1. Schematic of the disaggregation approach to calculate the new observation. In this example the model state has nine "pixels," and the coarse observation has just one value for this same area. Each of the pixel locations is labeled with a number from one to nine. These are used to indicate the locations of the samples in steps 4 and 5. A full description of the approach is given in the main text.

finest-resolution information. The approach is here after referred to as "disaggregation" as the coarse-scale observation is divided up into constituent parts, as determined by the fine-scale variability.

[10] In a pilot study we trialed data assimilation schemes using disaggregated observations that consisted of per pixel values for the subpixel variance and skew of the coarse-resolution observations. These disaggregated observations were assimilated via an appropriate observation operator into the data assimilation scheme. This observation operator took the form of a skew and variance of the model state relating to same spatial area as the observation. However, the performance of these implementations was found to be poor. Notwithstanding the fact that work could possibly be done to improve these approaches, they will still be limited to skew normal, or similar, subpixel observations distributions. In many ecosystems, where the distributions are more complex (e.g., multimodal) this limit could present real challenges. The disaggregation approach we outline is not limited to a given class of distributions and does not (necessarily) require any additional information to these approaches.

[11] The coarse EO is disaggregated to the high spatial resolution of the model. We assume that the spatial resolution of the model has been appropriately chosen to be capable of correctly representing nonlinear processes within the system. The disaggregated observation will possess the mean from the coarse observation, the spatial information from the model state and a prescribed PDF. The origins of this PDF could be from (infrequent) fine-resolution satellite or airborne observation, a detailed field study or "expert knowledge."

[12] In the following example (see Figure 1) we demonstrate the disaggregation procedure on a 3 by 3 pixel model state and a single coarse observation covering the same area is assimilated. Arbitrarily chosen PDFs are used to illustrate the approach.

[13] 1. For step 1, extract current model state and coarse observation of the system state, X. If needed, apply a suitable model operator to the model state (not done in this example). Index the location of each element in the model state, that is, $n = 1$ to 9. In the example the n model states have been drawn from a normal distribution with a mean (μ) = 5 and a standard deviation (σ) = 1. In this example we assume we have a coarse observation of value 7.

[14] 2. For step 2, assign a PDF to coarse observation of X. In this example, $\sigma = 1.5$ is picked for the PDF (the actual source of this PDF is discussed in detail later).

[15] 3. For step 3, randomly draw n samples from the observation PDF. The observation PDF of X is now represented by n sampled values.

[16] 4. For step 4, sort the n model states according to their values of X.

[17] 5. For step 5, assign the locations of the model states to the n observation samples according to the order of the numerical sorted model and observation values.

[18] 6. For step 6, reassemble the observation. The new disaggregated observation has the same spatial distribution

as the model state, the mean of the coarse observation, and the assigned PDF. This is referred to as a "disaggregated" observation, owing to the fact that it is no longer a pure observation. This disaggregated observation can now be used as a normal measurement in the data assimilation scheme.

[19] In the context of the particle filter the disaggregation was performed on the particle mean in these experiments, rather than on each individual particle. Consequently, irrespective of the number of particles used in the analysis the disaggregation was only performed once per observation. Using the particle mean as an approximation of the distribution's expected value imposes an assumption about the underlying distribution which is appropriate in this case, more generally however, it will be necessary to use other estimators of the expected value to avoid bias.

2.3. Demonstration Data Set

[20] The data assimilation analysis, in many ways, represents the sum of all our knowledge (i.e., about the model processes, observations, initial states, uncertainties and covariance). Therefore it can be tricky to assess the performance of data assimilation analyses, particularly when no independent prediction is being generated, as is the case in this example. For this reason, we first generate a realistic demonstration "truth," from which we can draw observations. This approach has been used before in data assimilation studies and allows the performance of the data assimilation to be assessed against a known "truth" [e.g., *Fox et al.*, 2009; *Trudinger et al.*, 2008].

[21] The demonstration data set is based on a normalized difference vegetation index (NDVI) map of Abisko, Sweden (68°21′N, 18°49′E) gathered from an aircraft flyover. The flyover took place on 17 July 2005 and was flown by the Natural Environment Research Council's (NERC) Airborne Research and Survey Facility (ARSF) aircraft. The ARSF aircraft used a Daedalus 1268 Airborne Thematic Mapper (ATM) multispectral scanner. The resolution of the image is 4 by 4 m. A section of this image 512 by 512 m, or 128 by 128 pixels, was used in this study.

[22] To provide the temporal variability associated with seasonal changes in phenology, the NDVI map was scaled according to observations from a nearby NDVI sensor (Skye Instruments, Powys, UK) mounted on a 3 m tower. NDVI records were available at 30 min intervals during 2007–9. After filtering for erroneous data points (NDVI < 0.4 or >0.8), we smoothed the NDVI time series using a seven day running mean window for the growing season of 123 days (May till August 2007). The NDVI time series was used as a gain factor to temporally extrapolate the NDVI map to form a demonstration data set, an hourly time series of NDVI maps. The gain was set to be unity on the day of year (17 July) that the aircraft map was acquired. The time series of NDVI maps was then converted to leaf area index (LAI) using an exponential relationship described by *van Wijk and Williams* [2005]. From these LAI and NDVI time series, fine-resolution maps, we drew incomplete and aggregated observations of NDVI.

2.4. Modeling Net Ecosystem Exchange of Carbon

[23] The net ecosystem exchange of carbon (NEE) was calculated from respiration and gross primary production (GPP) estimates. GPP and respiration were calculated by a simple ecosystem model driven by time series of downwelling photosynthetic photon flux density (PPFD), air temperature and LAI [*Shaver et al.*, 2007]. In *Shaver et al.*'s [2007] work, model GPP is calculated as a function of the light-saturated photosynthetic rate per leaf area, the Beer's law extinction coefficient, the initial slope of the light response curve, the top of canopy PPFD and LAI. Using the second of three functional forms in *Shaver et al.*'s [2007] paper, respiration is calculated as a function of respiration rate at 0°C, the air temperature, an empirical fit coefficient and LAI. We used parameters optimized for a wide range of Arctic vegetation assuming an extinction coefficient of 0.5 [*Shaver et al.*, 2007, Table 5]. PPFD and air temperature came from meteorological stations within the aircraft image. In this manner, cumulative GPP, respiration and NEE estimates could be calculated using LAI from the data assimilation analysis and compared to the "true" values calculated using the demonstration LAI data set.

2.5. General Data Assimilation Setup

[24] The model forecast step used a "zero-order" model of LAI, where the LAI at time t was simply the LAI at $t-1$ with the addition of the stochastic model noise at t, n_t:

$$\frac{\delta LAI}{\delta t} = n_t. \tag{1}$$

Each of the 16384 (i.e., 128 by 128) pixels were treated as a completely separate data assimilation, apart from the disaggregation of coarse observations. Consequently, no error covariance matrix was required as only a single variable comprised the state vector. While the model state was LAI, NDVI observations were assimilated and a model operator was used to translate the LAI model state into NDVI. This model operator was the same relationship used before to convert between LAI and NDVI [*van Wijk and Williams*, 2005].

[25] For each of the individual assimilations 250 particles (i.e., 250 particles per pixel and therefore 4,096,000 for the whole analysis) were used, though in tests very similar results were obtained with an order of magnitude fewer particles. The assimilations were initialized with $LAI_{t=0} = 0$ to avoid imposing any inherent spatial distribution on the assimilation. The alternative of using the mean value for the scene could have used, however the use of $LAI_{t=0} = 0$ conveniently reveals the rate at which the ensemble converges with observations. Convergence takes approximately five days (Figure 2). A lower bound was imposed that set negative model forecasts to be zero. The total length of the assimilations were 2952 steps, comprising of 24 h steps for 123 days, covering the growing season for a sub-Arctic environment. Model noise was set to have a variance of 0.0075 ($\sigma = 0.09$) and the observation uncertainty variance was set at 0.001 ($\sigma = 0.03$). In a synthetic study the correct choice of these parameters, and particularly the observation uncertainty, is somewhat unclear as the demonstration data represents the uncontaminated "truth." In this study the uncertainties were chosen so the data assimilation analysis had the freedom to track the observations, but at the same time be sufficiently constrained to avoid the being artificially constrained by the lower bound for LAI. On a stan-

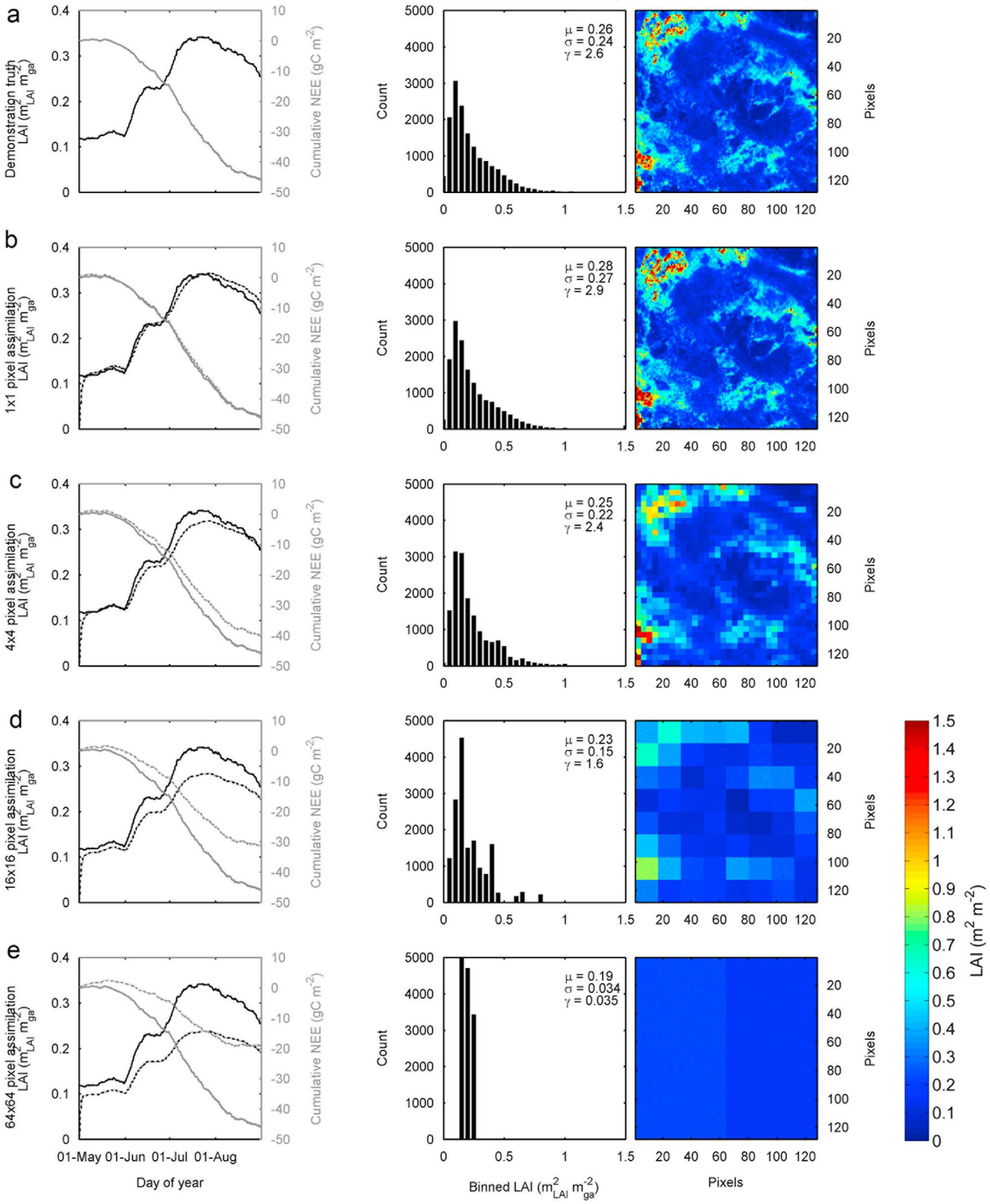

Figure 2. (a) Demonstration data, consisting of the mean LAI and cumulative NEE throughout the season, the final PDF of LAI, and the LAI map. The mean (μ), standard deviation (σ), and skew (γ) of the final PDF are shown in the a_2 graph. (b–e) Data for 1 by 1 pixel, 4 by 4 pixel, 16 by 16 pixel, and 64 by 64 pixel standard data assimilation analyses, respectively. The data assimilation analyses used the mean NDVI for the observation and did not use the disaggregation approach.

dard desktop computer an analysis took approximately one hour to complete.

[26] Instead of deriving a PDF from the fine-scale observations and randomly drawing from this PDF (steps 2 and 3) we simply use the fine-scale observations that were aggregated to form each coarse-scale observation. This is possible owing to the particular setup of our analysis and avoids the contrived step that would otherwise be necessary; the implications of this are discussed later. When using direct field measurements, the samples would be used to fit a PDF from which to draw. This allows field observations to be used to fit the PDF that are not collocated with the model grid.

2.6. Specific Data Assimilation Setup

[27] A "standard" data assimilation analysis was repeated for NDVI observation resolutions of 1 by 1 pixel, 4 by 4 pixel, 16 by 16 pixel, and 64 by 64 pixel; for example, for the 16 by 16 pixel resolution case, 64 observations covered the whole 128 by 128 pixel study region. In the standard analysis, the mean NDVI value for each observation resolution was assimilated. One NDVI observation was assimilated at noon of each day, on the remaining 23 h of each day no data were assimilated. That is on 96% of time steps no observations were assimilated and, unconstrained, the variance of the particle ensembles increased for these periods. The scheme functioned on a subdiurnal time step to allow instantaneous fluxes to be calculated using the NEE model [*Shaver et al.*, 2007].

[28] The disaggregation data assimilation analysis repeated the set of analyses performed for the standard data assimilation with the inclusion of the disaggregation methodology. Then using the assimilation of the 16 by 16 pixel observations as a bench mark, two further analyses were performed. The first additional analysis dealt with the case where coarse-resolution observations and high-resolution imagery could be combined and the second where the grid on which the observations were distributed shifted from one observation time to the next.

[29] Specifically, the first additional analysis simulated the case where coarse (MODIS) observations were being disaggregated using PDFs derived from a field survey; however, on one particular day, high-resolution imagery was also available. The assimilation was run as a repeat of the previous 16 by 16 pixel disaggregation assimilation, but with the inclusion of high-resolution (1 by 1 pixel) NDVI observations assimilated at 1000, 1100, 1200, 1300, and 1400 LT on day 148 (four weeks into the assimilation). Multiple high-resolution observations were assimilated in order that the assimilation analysis could converge with them.

[30] The second additional analysis was again based on the 16 by 16 pixel data assimilation runs with disaggregation and tested the impact of assuming that the grid on which each subsequent observation falls was not exactly collocated with the previous observations' grid. This crudely simulated the case where the position of satellite observation pixels is known but varies between each time step by some small amount. This is analogous to the way MODIS products are generated [*Wolfe et al.*, 1998]. In this case the coarse grid, on which the 16 × 16 pixel NDVI observations were drawn, was allowed to shift by 0 to 15 individual pixels in both dimensions.

3. Results

3.1. Standard Data Assimilation Performance

[31] The standard data assimilation did not use the disaggregation approach. The analysis was initialized at a LAI of zero and so did not reflect the initial distribution of the observations. The assimilation took approximately five days to reach the mean of the "true" LAI, though if a more realistic (than zero) initial LAI had been specified this delay could be eliminated (Figure 2, b_1 graph). All analyses captured the form of the seasonality in the mean LAI, but with approximately two to three days lag, however the magnitude of the analysis LAI was lower than the "true" area mean LAI which peaked at 0.34 m^2 m^{-2} (Figure 2, b_1, c_1, d_1, and e_1 graphs). This LAI underestimate increased with observation pixel size to a maximum underestimate of 33% with the 64 by 64 observation pixel. Additionally the PDF progressively collapsed, with an unrealistic reduction in both σ and skew (γ). This collapse was greatest for coarse observation resolutions. At a resolution of 64 by 64 pixels the final analysis PDF had $\mu = 0.19$, $\sigma = 0.034$ and $\gamma = 0.035$ (Figure 2, e_2 graph) compared to the demonstration data set values of $\mu = 0.26$, $\sigma = 0.24$ and $\gamma = 2.6$ (Figure 2, a_2 graph). Features larger than the resolution of the NDVI observations were still recognizable; however, at subobservation scales, variability was minimal (Figure 2, c_3, d_3, and e_3 maps). At observations scales other than 1 by 1 pixel the analysis cumulative NEE did not reproduce the "true" cumulative uptake of carbon of −45.9 gC m^{-2} for the period. At 1 by 1 pixels the cumulative NEE was over estimated by 1% (Figure 2, b_1 graph), at 4 by 4 pixels the underestimate was 12% (Figure 2, c_1 graph), at 16 by 16 pixels the underestimate was 32% (Figure 2, d_1 graph), and with 64 by 64 pixel observations the "true" cumulative NEE uptake was underestimated by 58% (Figure 2, e_1 graph). For the same period the "true" cumulative GPP was 153.9 gC m^{-2}, at 1 by 1 pixels the cumulative GPP was within 0.5%, at 4 by 4 pixels the underestimate was 5%, at 16 by 16 pixels the underestimate was 13%, and at 64 by 64 pixels the underestimate was 24%. The "true" cumulative respiration was 108.0 gC m^{-2}, at 1 by 1 pixels the cumulative respiration was within 0.2%, at 4 by 4 pixels the underestimate was 2%, at 16 by 16 pixels the underestimate was 6%, and at 64 by 64 pixels the underestimate was 10%.

3.2. Disaggregation Data Assimilation Performance

[32] The full suite of analyses was repeated with the inclusion of the disaggregation methodology. Again the analysis was initialized at a LAI of zero and takes approximately five days to reach the mean of observations (Figure 3, b_1, c_1, d_1, and e_1 graphs). All observation resolutions produced near identical temporal evolutions of LAI, with the two to three day lag, and distributions of LAI with identical means, standard deviations and skews (Figure 3, b_1, c_1, d_1, and e_1 graphs). Excluding the initial five day period, the maximum difference between the composite data set LAI and the analysis was 10%. This difference was similar for all observation resolutions and was the result of the analysis

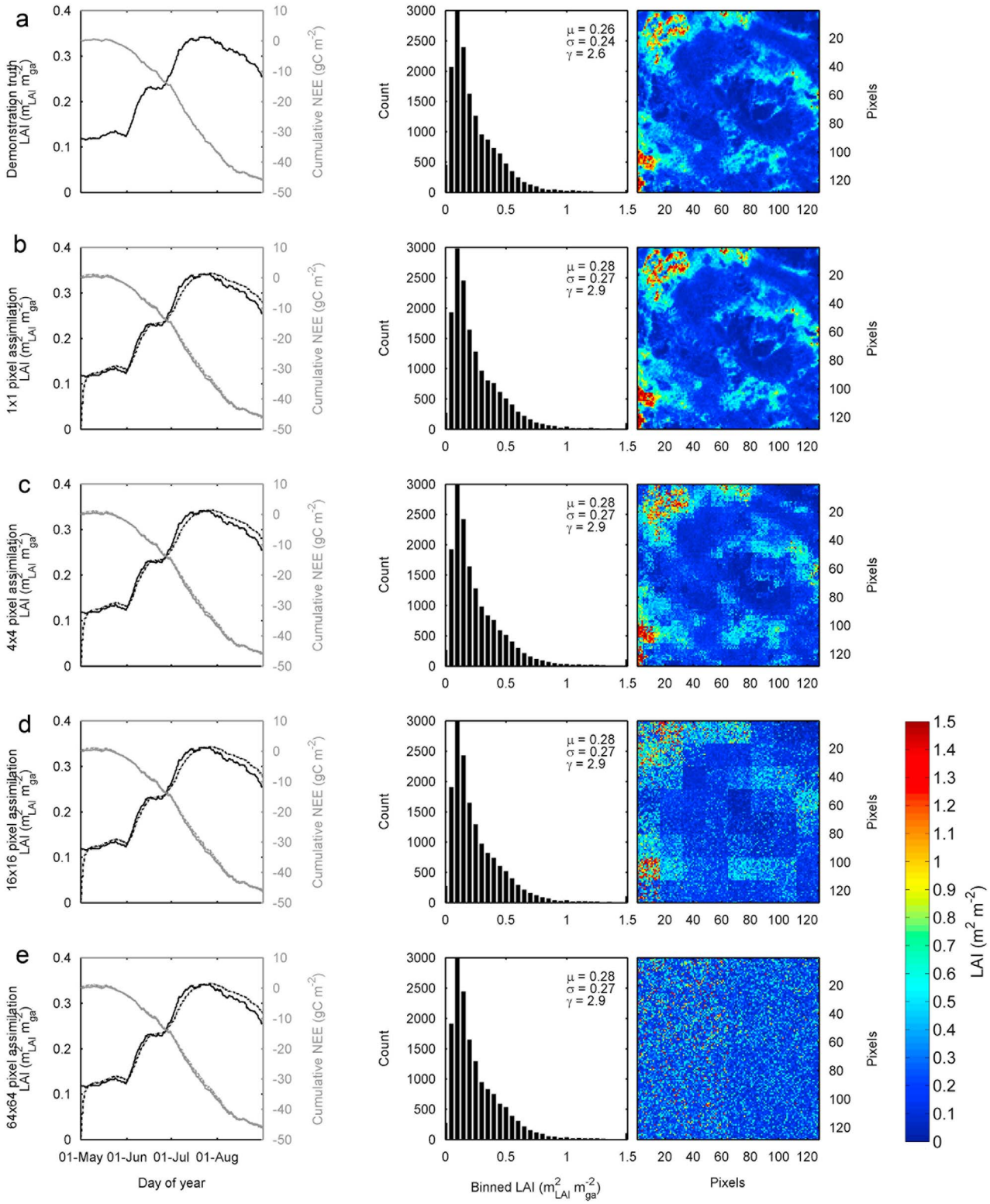

Figure 3. (a) Demonstration data, consisting of the mean LAI and cumulative NEE throughout the season, the final PDF of LAI, and the LAI map. The mean (μ), standard deviation (σ), and skew (γ) of the final PDF are shown in the a_2 graph. (b–e) Data for 1 by 1 pixel, 4 by 4 pixel, 16 by 16 pixel, and 64 by 64 pixel disaggregation data assimilation analyses, respectively. The analyses all used the disaggregation approach to assimilate the NDVI observations.

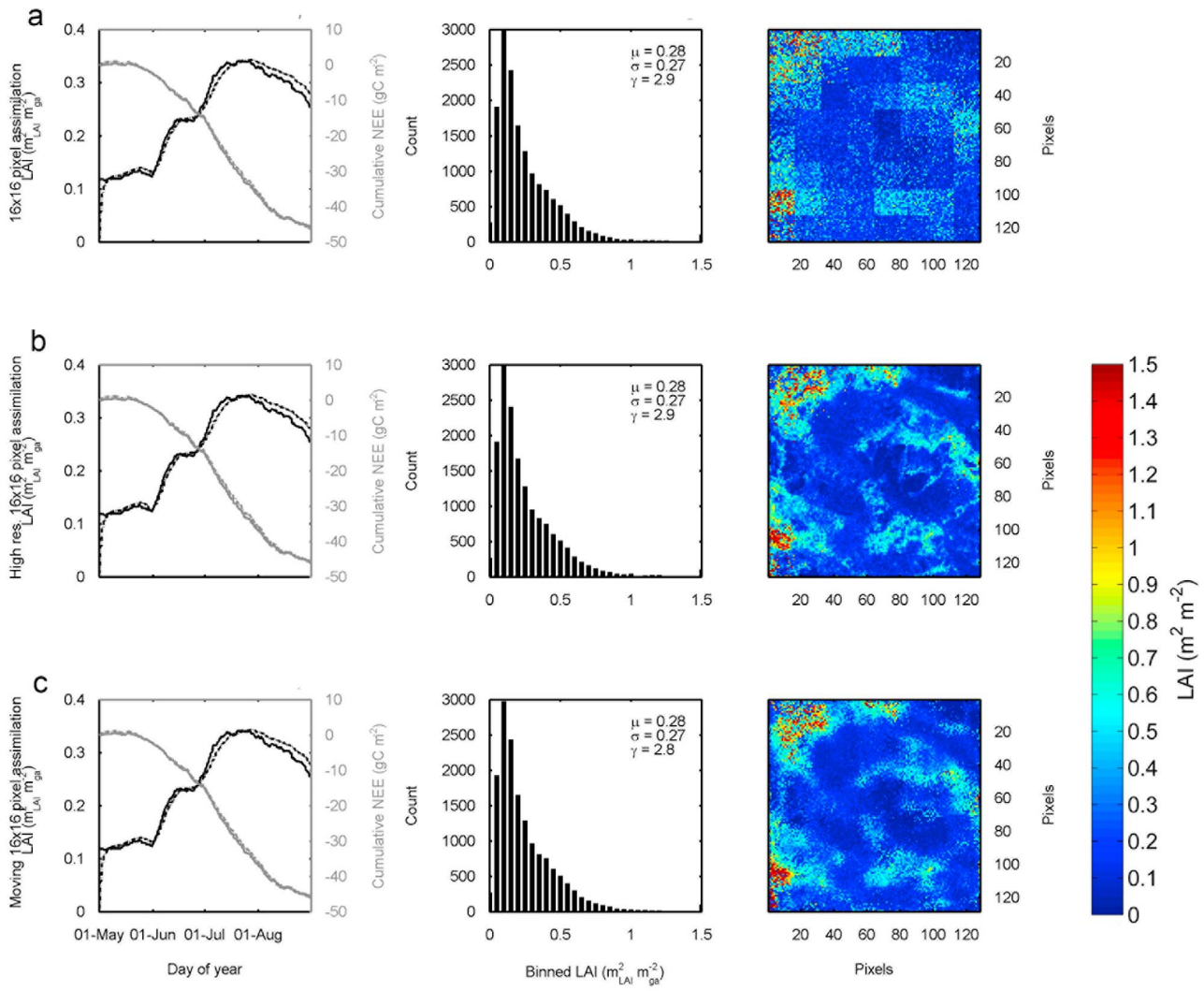

Figure 4. (a) Standard 16 by 16 pixel data assimilation analysis, consisting of the mean LAI and cumulative NEE throughout the season, the final PDF of LAI, and the LAI map. Figure 4a is the same as Figure 3d. The mean (μ), standard deviation (σ), and skew (γ) of the final PDF are shown in the a_2 graph. (b) The 16 by 16 pixel (with additional high-resolution NDVI "snap shot") data assimilation analysis. (c) The 16 by 16 data assimilation analysis, where successive NDVI observations shift in location rather than being collocated between observation times.

lagging behind the demonstration data set during periods of increasing LAI. The analyses overestimated the "true" cumulative NEE of −45.9 gC m^{-2} by 1% for all observation resolutions. Similarly the analysis GPP estimates were all with 0.5% of the "true" cumulative GPP of 153.9 gC m^{-2} and respiration estimates were all within 0.2% of the "true" cumulative respiration of 108.0 gC m^{-2} All analyses reproduced the final PDF closely, with $\mu = 0.28$, $\sigma = 0.27$ and $\gamma = 2.9$ compared to the demonstration data set values of $\mu = 0.26$, $\sigma = 0.24$ and $\gamma = 2.6$ (Figure 3, a_2, b_2, c_2, d_2, and e_2 graphs). The 1 by 1 pixel assimilation reproduced the spatial distribution very closely (Figure 3, b_3 map). As the observation scale coarsens so does the reduction in spatial detail (Figure 3, c_3, d_3, and e_3 maps). This drop in analysis resolution is directly linked to the observation resolution, with features finer than the observation not being resolved.

3.3. Disaggregation Data Assimilation Performance With Fine Spatial Resolution and Shifting Observations

[33] Using the 16 by 16 pixel data assimilation runs with disaggregation as a benchmark (Figure 4a), we tested the impact of adding in high-resolution observations on a single day. In this case the seasonality, and PDFs are very close to the first 16 × 16 data assimilation, but the final LAI map has retained more spatial information (Figure 4b). Cumulative NEE, GPP and respiration estimates were unchanged. Estimation of the final PDF improved and the analysis had identical μ, σ and γ to that of the demonstration data set (Figure 4, b_2 graph).

[34] Testing the impact of assuming that the grid on which each subsequent observation falls was not exactly collocated with the previous observations' grid showed both the seasonality and the final PDF agreed extremely closely with the

demonstration data set, with only the γ differing by 0.01 (Figure 4, c_1 and c_2 graphs). The spatial resolution was greatly improved to a level that (visually) appears somewhat similar to the 4 by 4 pixel data assimilation (Figure 4, c_3 map). Cumulative NEE, GPP and respiration estimates were unchanged.

4. Discussion

[35] There is a compelling case being made for a framework to integrate all available observations with spatially and temporally explicit ecosystem models [*Raupach et al.*, 2005; *Tang and Zhuang*, 2008]. Observations not only differ in the quantity measured, but also in spatiotemporal resolution and extent. Data assimilation has been proposed as a natural framework with which the integration of models and measurements can be formalized. However, in order to achieve this integration with data assimilation, a consistent and unbiased method for combining models with multiresolution spatiotemporal data is needed. Any such methodology needs to manage the issues of scaling in heterogeneous ecosystems highlighted by *Stoy et al.* [2009]. This is expected to be particularly important for highly nonlinear processes, and studies have shown a greater effect on fluxes of carbon rather than latent and sensible heat fluxes [*Kimball et al.*, 1999; *Stoy et al.*, 2009; *Wood and Lakshmi*, 1993]. However, some caution should be employed when comparing these results as the processes and scales of observation vary.

[36] The disaggregation framework that we propose provides a flexible and robust method for combining fine-resolution (infrequent) and coarse-resolution (frequent) observations with terrestrial ecosystem models. There are no implicit assumptions about the PDF used in the disaggregation routine and so the approach can work with nonnormal distributions and even multimodal PDFs. The routine has intentionally been formulated to be easily implemented in a wide range of data assimilation schemes.

[37] Using a demonstration data set we evaluated the performance of the disaggregation approach. The demonstration data set used was temporally smoothed, by the seven day windowing of the tower NDVI time series. This smoothed data set can be expected to be easier to assimilate than a noisy, unsmoothed data set (if it existed). However, using the composite data allowed the performance of the assimilations to be assessed relative to a known "truth."

[38] Owing to the particular setup of this study, we did not perform "step 3" of the disaggregation approach; the random drawing of samples from the PDF. While this could be seen as a shortcut that reduced noise by reusing the high-resolution demonstration data sets PDF, it remains a logical step. When high-resolution imagery is used to provide the PDF, the same approach (missing out "step 3") should be used. In this study this step is particularly important, as the PDF is not a normal distribution (e.g., Figure 2, a_2 graph). Alternatively, when direct field studies and/or expert knowledge forms the basis of the PDF, the PDF would normally be better described than by, for example, the 16 samples in the 4 by 4 pixel observations. The effectiveness of the approach would then depend on how well the PDF was described by the field study, and the spatial extent for which the PDF can be considered representative. The disaggregation approach will not compensate for poorly described PDFs, nor can it account for a PDF's lack of spatial representativeness (i.e., trying to apply a PDF derived from one biome, to another ecologically distinct biome).

[39] The use of a zero-order model for LAI introduced a two to three day lag in the analysis mean. This lag is to be expected with such a simple LAI model, as updates to the model state only came through the assimilation of observations. This model was picked to illustrate the benefits of the disaggregation process clearly, however for general applications it might be more reasonable to use a model with mechanistic phenology, which would eliminate much of this lag. Indeed for assimilations relying on less frequent observations, a process-based model would likely be required.

4.1. Biases and the Standard Data Assimilation of Coarse Observations

[40] Without the disaggregation the mean (μ), standard deviation (σ) and skew (γ) were not preserved in the analysis (Figure 2, a_2, b_2, c_2, d_2, and e_2 graphs). These deviations were manifested as an underestimate of the mean LAI, a collapse of the PDF and an underestimate of the NEE magnitude. As the observations become coarser the effect increases until at a resolution of 64 by 64 pixels the carbon uptake was underestimated by the data assimilation analysis by 58% (Figure 2, e_2 graph). The 58% (26.8 gC m^{-2}) NEE underestimate is composed of a GPP underestimate of 24% (37.5 gC m^{-2}) and a respiration underestimate of 10% (10.7 gC m^{-2}). Thus the inability of the standard assimilation to deal with nonlinear processes occurs in both the production and respiration of carbon. In both percentage and absolute terms the underestimate is larger for GPP than for respiration. This GPP error could be avoided by exploiting the broadly linear relationship of GPP with remotely sensed fraction of absorbed photosynthetically active radiation (fAPAR) products. However, NEE estimates would still be biased owing to errors in respiration. Furthermore, when considering more detailed ecosystem models which explicitly allocate GPP, a nonlinear relationship between the carbon invested in resources for photosynthesis and fAPAR would be required. This nonlinear relationship, as well as other nonlinear responses (such as the significant lag between GPP and subsequent heterotrophic respiration) would be expected to result in biases when assimilating coarse observations in heterogeneous ecosystems with standard approaches.

[41] The coarsest resolution we consider (256 m by 256 m) approximately matches the finest resolution available for MODIS products, and is finer than the 1 km by 1 km resolution products frequently used in terrestrial ecosystem studies. At resolutions coarser than those considered in this study the problem is expected to be worse. However, the effect can be expected to vary with the specific sub-observation heterogeneity and the nonlinearity of the key processes and model operators. In a similar analysis, *Stoy et al.* [2009] found the flux of carbon to change sign (from a sink to a source) with varying observation scales.

4.2. Improvements With the Disaggregation Approach to Data Assimilation

[42] Using a demonstration data set, the performance of the disaggregation method has been shown to be robust

(Figure 3) and to avoid the scaling issues often associated with using coarse observations (Figure 2) [*Stoy et al.*, 2009]. The disaggregation method successfully assimilated the observations such that the mean (μ), standard deviation (σ) and skew (γ) of the observations were preserved in the data assimilation analysis. Contrary to the example without the application of the disaggregation, the performance of the assimilation was preserved irrespective of the observation resolution (Figure 3). The disaggregation approach successfully estimated the cumulative NEE, GPP and respiration terms. From the spatial maps presented, it can be seen that while the PDF of the observations was preserved, no spatial information was imposed below the size of observations (Figure 3, a_3, b_3, c_3, d_3, and e_3 maps). *Chen et al.* [2010] also blended (infrequent) fine-resolution observations (LANDSAT) and (frequent) coarse-resolution MODIS imagery to obtain a temporally frequent high-resolution (30 m) data set. However, our results indicate that all else being equal the use of LANDSAT imagery, without the disaggregation, at 30m would result in an underestimate of cumulative NEE somewhere between 12% (4 by 4 pixels, 16 by 16 m) and 32% (16 by 16 pixels, 64 by 64 m).

4.3. Performance of the Disaggregation Approach With Fine Spatial Resolution and Shifting Observations

[43] The performance of the assimilations is improved with the addition of infrequent high-resolution NDVI imagery (Figure 4, b_2 and b_3 graphs). The high-resolution imagery imprinted the model state with finer-resolution spatial information and the final PDF μ, σ and γ were slightly closer to the demonstration data set values. Spatial information was propagated forward in time by the model state, though this information will degrade with time after a high-resolution observation, with the uncertainty determined by the model noise. This performance increase will be of benefit for field studies where infrequent (e.g., airborne, IKONOS) imagery is available, but at an insufficient frequency to capture the temporal dynamics of the ecosystem. However, the analysis presented here was not sufficient to determine to what extent multiresolution data of different types (e.g., NDVI and surface moisture) can be combined with benefits to spatial resolution. Further studies are required, but it is likely that the benefit of combining multitype, multiresolution observations will be determined by the covariances between the data types and their combined ability to constrain key model states.

[44] Combining shifting observations allowed the assimilation to improve the spatial information in the analysis (Figure 4, c_3 map). Considered over several time steps, the shifting observation grid permitted a finer-resolution constraint to be placed on the model state which translated into improved spatial resolution. This result makes it attractive to consider noncollocated observations from multiple satellites, even if they are of a similar resolution, provided that their geolocation is accurately known.

4.4. Future Challenges

[45] Considering the application of the disaggregation approach to real-world ecosystems, it quickly becomes apparent that there are significant challenges to be addressed:

4.4.1. Challenge One: Determining the Subpixel PDF

[46] The disaggregation method we propose allows coarse observations to be combined with subpixel PDFs. However, it is obvious that without knowing, or assuming, subpixel information we cannot account for processes at scales smaller than our observation resolution, potentially resulting in prediction biases. In reality, this information could be hard to obtain, but fortunately there are a number of possible sources. We suggest that the required PDFs can be spatially extrapolated from local fine-resolution information, and applied to a wider area. The PDFs could also be temporally extrapolated from infrequent fine-resolution imagery (e.g., from aircraft and satellites), as we have done in this study. Alternatively, this approach allows the PDF to be derived from field surveys, even when the sampling design does not permit a "map" to be drawn. This ability to use field surveys represents a significant advantage over similar, image only, approaches [*Chen et al.*, 2010].

4.4.2. Challenge Two: Determining the Subpixel Observation Uncertainty

[47] When considering real observations it is as yet unresolved how to specify the observation uncertainties for the disaggregated observation. By definition the disaggregated observations must be at least as uncertain than the original coarse observation. In particular, there is an uncertainty associated with the coarse-scale observation (that provides the mean for the disaggregated observation) and another uncertainty associated with determining the PDF itself. The first uncertainty is common to all data assimilation approaches; see section 4.4.3. The second uncertainty, which is unique to this approach, is somewhat mitigated by the nature of the uncertainty. For instance if we sample a normal distribution with $\mu = 0$ and $\sigma = 1$, and each sample has a measurement uncertainty of $\mu = 0$ and $\sigma = 0.1$, the σ of the PDF will, on average, be overestimated by just 0.5%. This is likely to be much lower than the uncertainty on the coarse observation. However, the derivation of these uncertainties will be dependent on the observation, the quality controls imposed on the observations, and the purpose of the analysis.

4.4.3. Challenge Three: Dealing With Biases in Models and Real-World Observations

[48] Even ignoring issues of scaling, models and measurements can exhibit significant biases, as is the case with any data assimilation scheme. Research in this area exists [*Dee*, 2005; *Dee and Da Silva*, 1998], but working at multiple scales brings new challenges. The derivation of remote sensing products often involves complex inverse modeling strategies that may not transfer well from scale to scale. The MODIS LAI products, for example, use the inversion of a complex radiative transfer scheme that, in part, relies on reflectance data being acquired at differing view angles over a relatively short period of time (around 8 days). It is unlikely that sufficient data will be acquired over a short enough period of time by, for example, Landsat to repeat this analysis. Thus methodological biases might exist in the derivation of the observation products. Furthermore, empirical approaches to estimating LAI, such as the one used here will not hold generally over a wide range of cover types or view and illumination geometries. A more elegant approach to resolve these issues would be to forward model reflectance from the process model, using an observation

operator, and assimilate actual reflectance data [*Quaife et al.*, 2008]. The operator can be made consistent across scales, wave bands and arbitrary view and illumination geometries and will consequently remove bias between the different scales. A noteworthy study is that by *Roy et al.* [2008] in which MODIS and Landsat data are combined using kernel driven Bidirectional Reflectance Distribution Function (BRDF) models to negate differences between the position of the satellite and the sun. This presents a simple and elegant step via which some of these goals may be achieved.

[49] In this manuscript we have used a single model to describe the production of tundra, where productivity is determined by LAI and not cover type [*Shaver et al.*, 2007]. To extend this approach to land-surface exchange models with plant functional types (PFT) it is likely that the model operator would have to be modified to cope with separate PDFs for each PFT. Furthermore the use of spatial correlations, thematic information (e.g., field boundaries) and contexture approaches [*Chen*, 1999] could be exploited to benefit the data assimilation process.

5. Conclusions

[50] In our data assimilation disaggregation method, frequent, coarse-resolution observations are combined with an estimate of their subpixel probability distribution function (PDF) and the fine-resolution model state to produce a fine-resolution disaggregated observation that can then be assimilated normally. The subpixel PDF can be derived from a variety of sources, either from (infrequent) fine-resolution Earth observation, or from detailed field studies. We demonstrate the data assimilation disaggregation method by assimilating normalized difference vegetation index (NDVI) observations into a zero-order model of leaf area index (LAI) for a 512 by 512 m area. Using the data assimilation analysis LAI, and meteorological observations, we predict the uptake of carbon by the system. The methodology is shown to be extremely robust and clearly out performs standard approaches that do not make use of the disaggregation method. Using the data assimilation disaggregation approach results in a 1% overestimate of carbon uptake, compared to the 58% underestimate of carbon uptake that occur with the standard assimilation of coarse (256 m by 256 m) observations. The approach is easily implemented in most data assimilation schemes and benefits from combining multiple observations at differing spatial and temporal resolutions.

[51] **Acknowledgments.** The Natural Environment Research Council (NERC) funded this work through the National Centre for Earth Observation (NCEO) and the Centre for Terrestrial Carbon Dynamics (CTCD). We are grateful to B. Huntley and R. Baxter for access to the Natural Environment Research Council's (NERC) Airborne Research and Survey Facility (ARSF) spatial maps of NDVI; C. Llyod, J. Evans, and R. Harding for access to meteorological data; and also M. Disney and A. Prieto-Blanco for providing processed NDVI data gathered as part of the NERC Arctic Biosphere Atmosphere at Multiple Scales (ABACUS) project. Finally, the authors would like to express their gratitude to the anonymous reviewers for their valuable comments.

References

Bayes, T. (1763), An essay towards solving a problem in the doctrine of chances, *Philos. Trans. R. Soc. London*, *53*, 370–418, doi:10.1098/rstl.1763.0053.

Chen, B. Z., J. M. Chen, G. Mo, C. W. Yuen, H. Margolis, K. Higuchi, and D. Chan (2007), Modeling and scaling coupled energy, water, and carbon fluxes based on remote sensing: An application to Canada's landmass, *J. Hydrometeorol.*, *8*(2), 123–143, doi:10.1175/JHM566.1.

Chen, B., Q. Ge, D. Fu, G. Yu, X. Sun, S. Wang, and H. Wang (2010), A data-model fusion approach for upscaling gross ecosystem productivity to the landscape scale based on remote sensing and flux footprint modelling, *Biogeosciences*, *7*(9), 2943–2958, doi:10.5194/bg-7-2943-2010.

Chen, J. M. (1999), Spatial scaling of a remotely sensed surface parameter by contexture, *Remote Sens. Environ.*, *69*(1), 30–42, doi:10.1016/S0034-4257(99)00006-1.

Dee, D. P. (2005), Bias and data assimilation, *Q. J. R. Meteorol. Soc.*, *131*(613), 3323–3343, doi:10.1256/qj.05.137.

Dee, D. P., and A. M. Da Silva (1998), Data assimilation in the presence of forecast bias, *Q. J. R. Meteorol. Soc.*, *124*(545), 269–295, doi:10.1002/qj.49712454512.

Demarty, J., F. Chevallier, A. D. Friend, N. Viovy, S. Piao, and P. Ciais (2007), Assimilation of global MODIS leaf area index retrievals within a terrestrial biosphere model, *Geophys. Res. Lett.*, *34*, L15402, doi:10.1029/2007GL030014.

Dowd, M. (2007), Bayesian statistical data assimilation for ecosystem models using Markov Chain Monte Carlo, *J. Mar. Syst.*, *68*(3–4), 439–456, doi:10.1016/j.jmarsys.2007.01.007.

Evensen, G. (2003), The Ensemble Kalman Filter: Theoretical formulation and practical implementation, *Ocean Dyn.*, *53*, 343–367, doi:10.1007/s10236-003-0036-9.

Evensen, G. (2009), The Ensemble Kalman Filter for combined state and parameter estimation: Monte Carlo techniques for data assimilation in large systems, *IEEE Control Syst. Mag.*, *29*(3), 83–104, doi:10.1109/MCS.2009.932223.

Fletcher, B. J., M. C. Press, R. Baxter, and G. K. Phoenix (2009), Transition zones between vegetation patches in a heterogeneous Arctic landscape: How plant growth and photosynthesis change with abundance at small scales, *Oecologia*, *163*, 47–56, doi:10.1007/s00442-009-1532-5.

Fox, A., et al. (2009), The REFLEX project: Comparing different algorithms and implementations for the inversion of a terrestrial ecosystem model against eddy covariance data, *Agric. For. Meteorol.*, *149*(10), 1597–1615, doi:10.1016/j.agrformet.2009.05.002.

Jarvis, P. G. (1995), Scaling processes and problems, *Plant Cell Environ.*, *18*(10), 1079–1089, doi:10.1111/j.1365-3040.1995.tb00620.x.

Kimball, J. S., S. W. Running, and S. S. Saatchi (1999), Sensitivity of boreal forest regional water flux and net primary production simulations to sub-grid-scale land cover complexity, *J. Geophys. Res.*, *104*(D22), 27,789–27,801, doi:10.1029/1999JD900085.

Quaife, T., P. Lewis, M. De Kauwe, M. Williams, B. E. Law, M. Disney, and P. Bowyer (2008), Assimilating canopy reflectance data into an ecosystem model with an Ensemble Kalman Filter, *Remote Sens. Environ.*, *112*(4), 1347–1364, doi:10.1016/j.rse.2007.05.020.

Raupach, M. R., P. J. Rayner, D. J. Barrett, R. S. DeFries, M. Heimann, D. S. Ojima, S. Quegan, and C. C. Schmullius (2005), Model-data synthesis in terrestrial carbon observation: Methods, data requirements and data uncertainty specifications, *Global Change Biol.*, *11*(3), 378–397, doi:10.1111/j.1365-2486.2005.00917.x.

Roy, D. P., J. Ju, P. Lewis, C. Schaaf, F. Gao, M. Hansen, and E. Lindquist (2008), Multi-temporal MODIS-Landsat data fusion for relative radiometric normalization, gap filling, and prediction of Landsat data, *Remote Sens. Environ.*, *112*(6), 3112–3130, doi:10.1016/j.rse.2008.03.009.

Saatchi, S. S., R. A. Houghton, R. C. D. S. Alvala, J. V. Soares, and Y. Yu (2007), Distribution of aboveground live biomass in the Amazon basin, *Global Change Biol.*, *13*(4), 816–837, doi:10.1111/j.1365-2486.2007.01323.x.

Shaver, G. R., L. E. Street, E. B. Rastetter, M. T. Van Wijk, and M. Williams (2007), Functional convergence in regulation of net CO_2 flux in heterogeneous tundra landscapes in Alaska and Sweden, *J. Ecol.*, *95*(4), 802–817, doi:10.1111/j.1365-2745.2007.01259.x.

Spadavecchia, L., M. Williams, R. Bell, P. C. Stoy, B. Huntley, and M. T. van Wijk (2008), Topographic controls on the leaf area index and plant functional type of a tundra ecosystem, *J. Ecol.*, *96*(6), 1238–1251, doi:10.1111/j.1365-2745.2008.01424.x.

Stoy, P. C., M. Williams, M. Disney, A. Prieto-Blanco, B. Huntley, R. Baxter, and P. Lewis (2009), Upscaling as ecological information transfer: A simple framework with application to Arctic ecosystem carbon exchange, *Landscape Ecol.*, *24*(7), 971–986, doi:10.1007/s10980-009-9367-3.

Tang, J., and Q. Zhuang (2008), Equifinality in parameterization of process-based biogeochemistry models: A significant uncertainty source to the estimation of regional carbon dynamics, *J. Geophys. Res.*, *113*, G04010, doi:10.1029/2008JG000757.

Tang, J., and Q. Zhuang (2009), A global sensitivity analysis and Bayesian inference framework for improving the parameter estimation and prediction of a process-based Terrestrial Ecosystem Model, *J. Geophys. Res.*, *114*, D15303, doi:10.1029/2009JD011724.

Trudinger, C. M., M. R. Raupach, P. J. Rayner, and I. G. Enting (2008), Using the Kalman filter for parameter estimation in biogeochemical models, *Environmetrics*, *19*(8), 849–870, doi:10.1002/env.910.

van Leeuwen, P. J. (2009), Particle filtering in geophysical systems, *Mon. Weather Rev.*, *137*(12), 4089–4114, doi:10.1175/2009MWR2835.1.

van Wijk, M. T., and M. Williams (2005), Optical instruments for measuring leaf area index in low vegetation: Application in Arctic ecosystems, *Ecol. Appl.*, *15*(4), 1462–1470, doi:10.1890/03-5354.

Williams, M., P. A. Schwarz, B. E. Law, J. Irvine, and M. R. Kurpius (2005), An improved analysis of forest carbon dynamics using data assimilation, *Global Change Biol.*, *11*(1), 89–105, doi:10.1111/j.1365-2486.2004.00891.x.

Williams, M., et al. (2009), Improving land surface models with FLUXNET data, *Biogeosciences*, *6*(7), 1341–1359, doi:10.5194/bg-6-1341-2009.

Wolfe, R. E., D. P. Roy, and E. Vermote (1998), MODIS land data storage, gridding, and compositing methodology: Level 2 grid, *IEEE Trans. Geosci. Remote Sens.*, *36*(4), 1324–1338, doi:10.1109/36.701082.

Wood, E. F., and V. Lakshmi (1993), Scaling water and energy fluxes in climate systems: Three land atmospheric modeling experiments, *J. Clim.*, *6*(5), 839–857, doi:10.1175/1520-0442(1993)006<0839:SWAEFI>2.0.CO;2.

Zobitz, J. M., D. J. P. Moore, W. J. Sacks, R. K. Monson, D. R. Bowling, and D. S. Schimel (2008), Integration of process-based soil respiration models with whole-ecosystem CO2 measurements, *Ecosystems*, *11*(2), 250–269, doi:10.1007/s10021-007-9120-1.

T. C. Hill and M. Williams, School of GeoSciences, University of Edinburgh, Kings Bldgs., West Mains Rd., Edinburgh EH9 3JN, UK. (thill@staffmail.ed.ac.uk)

T. Quaife, School of Geography, University of Exeter, Peter Lanyon Bldg., Penryn, Cornwall TR10 9EZ, UK.